Effect of Cu modifier on the performance of CrO$_x$/Al$_2$O$_3$ catalysts for isobutane dehydrogenation

A.A. Salaeva, M.A. Salaev, G.V. Mamontov *

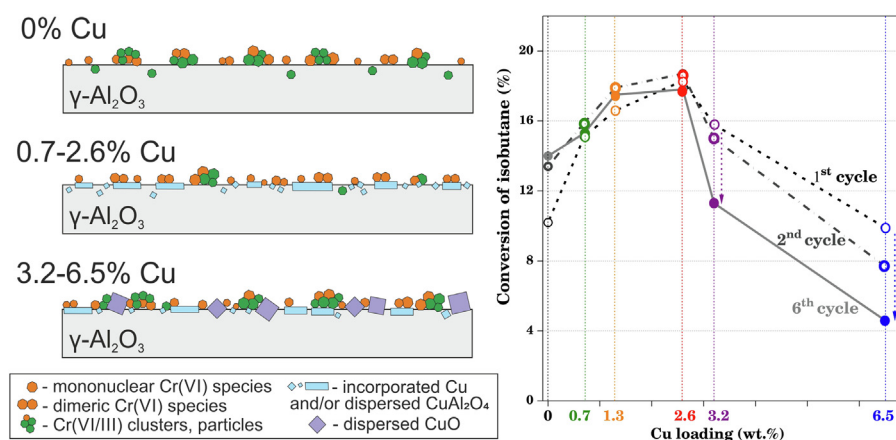*Tomsk State University, 36, Lenin ave., 634050 Tomsk, Russia*

HIGHLIGHTS

- Proper amounts of Cu enhance performance of CrO$_x$/Al$_2$O$_3$ in i-C$_4$H$_{10}$ dehydrogenation.
- Cu modifier stabilizes chromium as mono- and dimeric reducible Cr(VI) species.
- High Cu loadings reduce catalyst activity due to formation of dispersed Cu oxides.

GRAPHICAL ABSTRACT

ABSTRACT

The peculiarities of active surface formation and the effect of Cu modifier on the performance of CrO$_x$/Al$_2$O$_3$ catalysts in a fixed-bed isobutane dehydrogenation into isobutylene are considered using a series of model Cu-modified alumina supports (0.7–6.5% wt Cu) and CrO$_x$ catalysts on the basis thereof. The samples are characterized using a complex of physical-chemical methods, including low-temperature N$_2$ adsorption, STA, XRF, XRD, UV–vis DR, Raman spectroscopy and H$_2$-TPR. The modification of the alumina-chromia catalysts by a proper amount of copper is shown to enhance the catalyst activity. The catalyst with 2.6% wt Cu shows high conversion and selectivity towards isobutylene. The role of Cu modifier is connected with stabilizing of the active component mostly as monomeric and dimeric Cr(VI) species that can be reduced into the most active mononuclear and dimeric Cr^{3+} sites.

© 2019 Elsevier Ltd. All rights reserved.

1. Introduction

Isobutylene is among the most in-demand products of chemical industry and serves as a building block in manufacturing of various value-added products that include, but are not limited to, gasoline oxygenates (e.g., MTBE, ETBE, etc.), isooctane actively used as

functional additives to fuels, a number of polymers (e.g., poly-isobutylene, butyl rubber, etc.) used in manufacturing of tyres for vehicles as well as anti-oxidants, lubricants, adhesives, etc. (Geilen et al., 2014).

An increasing demand in isobutylene promotes new research focused on the development and intensification of catalytic technologies for its production. Various catalysts compositions were proposed for dehydrogenation of light alkanes (Sattler et al., 2014; Nawaz, 2015), including industrially implemented

composites based on Cr (Otroshchenko et al., 2017; Fridman and Xing, 2017a, 2017b; Fridman, 2010; Lamberov et al., 2017; Bugrova et al., 2015; Wang et al., 2018) and Pt-Sn (Dong et al., 2017; Liu et al., 2018; Tasbihi et al., 2007; Zhang et al., 2012) as well as the materials based on ZrO_2 (Zhang et al., 2018; Bugrova and Mamontov, 2018), Zn (Liu et al., 2018), Ga (Wang et al., 2016), Ni-Sn (Wang et al., 2016), Fe-Zn (Cheng et al., 2019), V (Rodemerck et al., 2017; Wang et al., 2018; Tian et al., 2016; Kharlamova et al., 2016), etc. Among the industrial catalysts for isobutane dehydrogenation, the CrO_x/Al_2O_3 catalysts have found wide applications, since they are cost-effective, and allow achieving high isobutylene yields, while keeping high selectivity and stability during several years (Fridman and Xing, 2017a). Industrial exploitation of alumina-chromia catalysts is carried out under hard process conditions comprising high process temperature (500–650 °C), repeated cycles of oxidative regeneration and reduction, local overheating, etc. (Pat, 2004). Given this, the catalyst should possess high thermal stability, high activity and selectivity at elevated temperatures.

To increase the effectiveness and productivity it is essential to develop the catalysts with improved exploitation characteristics. Various additives have been introduced into the composition of CrO_x/Al_2O_3 catalysts as modifiers or promoters. In most cases, alkali and alkali-earth metals are used to stabilize the structure of alumina support and provide the opportunity to control the acid properties of the catalyst surface by decreasing the concentration of Lewis acid sites (Al^{3+}) and/or increasing the amount of active Cr species (Sattler et al., 2014; Pat, 2004; Rombi et al., 2003; Pat. RU 2287366; Neri et al., 2004; Pat. RU 2349378) that exist as mononuclear redox Cr species and those chemically bound to alumina (Fridman and Xing, 2017b), non-redox and redox Cr(III) species that can be oxidized into Cr(V) and Cr(VI) during the regeneration stage, amorphous and crystalline Cr_2O_3 clusters (Fridman et al., 2016; Cavani et al., 1996; Vuurman et al., 1993), and Cr^{2+} species (Sattler et al., 2014). The modifiers that increase thermal stability include those based on boron, silicon (Pat. RU 2349378; Pat. RU 2350594; Bekmukhamedov, 2016), and tin (Pat. RU 2287366). Moreover, Zr, Fe and Si oxides allow stabilizing the phase composition and increasing the strength properties of the catalysts (Neri et al., 2004; Cabrera et al., 2008). The compounds that contain potassium (Rombi et al., 2003), calcium (Neri et al., 2004), nickel (Beccari and Romano, 2006), etc., are used to increase the catalytic activity and selectivity.

A number of patents for isobutane dehydrogenation catalysts (Pat. RU 2349378; Pat. RU 2350594; Pat, 2005) reports the modifiers based on Cu compounds that are widely used in other catalytic processes (Lindström et al., 2002; Fridman et al., 2004; Bahmani et al., 2016; Yashnik et al., 2015), while in the process under consideration copper is mostly used as a component of heat-generating material (Pat. US 9725380), and its catalytic properties are poorly discussed. The heat-generated material comprises α-Al_2O_3-supported copper oxides or Ca aluminate that are mixed with the main alumina–chromia catalyst and promote the heat release due to redox reactions of copper. The contact of the heat-generated material with the catalysts and high process temperature accompanied by the redox transitions of copper may lead to copper migration from the heat-generated material to the catalyst. Thus, the key question concerns a positive or negative effect of copper on the catalytic properties of CrO_x/Al_2O_3 catalyst during its long-time industrial exploitation in the Catofin process.

In our previous work (Merk et al., 2018) a combination of Cu and Zn modifiers was shown to improve the catalytic performance of CrO_x/Al_2O_3 catalysts for isobutane dehydrogenation into isobutylene independently on the introduction method. In Ref. (Salaeva et al., 2019) Cu modifier was shown to facilitate the activity growth of the alumina-chromia catalyst, while the introduction of Zn led to activity decrease. Contrary, in Ref. (Matveyeva et al., 2019) the introduction of Cu was shown to reduce the catalyst activity and increase the activation energy for isobutane dehydrogenation under kinetic conditions. Thus, the key challenge is to reveal the mechanism of Cu influence on the state of the active surface of CrO_x/Al_2O_3 catalysts, its changing in a series of repeated oxidative and reductive treatments as well as the nature, amount and catalytic activity of the active Cr species formed.

The present work is focused on the study of the effect of the content of Cu modifier on the performance of alumina-supported CrO_x catalysts for a fixed-bed isobutane dehydrogenation into isobutylene. Special attention is given to studying of textural characteristics and redox properties of the modified supports that contain 0.7–6.5% wt Cu as well as the peculiarities of formation of the active Cr sites on the catalyst surface.

2. Experimental

2.1. Synthesis of supports and catalysts

The precursor of γ-Al_2O_3, the industrial pseudoboehmite AlO(OH) (CJSC "Industrial catalysts", Russia), was obtained by precipitation of sodium aluminate by sulfuric acid (pH = 7–9) followed by washing from Na ions and drying at 120 °C overnight to remove physically bonded water. Copper modifier was introduced in the amount from 0.7 to 6.5% wt calculated per Cu during the wetness impregnation of the pseudoboehmite from water solution of Cu $(NO_3)_2 \cdot 3H_2O$ (99%, "ACROS organics"). The synthesized samples were subjected to drying at 120 °C for 12 h and calcination for 6 h in air at 750 °C. To obtain the catalysts with a monolayer distribution of active component, the modified supports were prepared using wetness impregnation method by water solution of CrO_3 (chemically pure, "Vecton", Russia) and KNO_3 (chemically pure, "Vecton", Russia) calculated per their content in the catalyst of 4.0 and 0.85% wt of Cr_2O_3 and K_2O, respectively. According to XRF data, the loadings of Cr and K were 3.7–3.8% wt and 0.8–0.9% wt, respectively, for all catalysts prepared (Table 1). The prepared catalysts were dried at 120 °C for 12 h and calcined in air for 6 h at 750 °C as the industrial catalysts for the Catofin process (Pat. US 20130072739).

Table 1
Characteristics of porous structure of modified supports and alumina-chromia catalysts.

Support	S_{BET},m²/g	V_{pore},cm³/g	Catalyst	S_{BET},m²/g	V_{pore},cm³/g	Composition of elements, % wt					
						Al	O	Cu	K	Cr	$\sum$
Al_2O_3	115	0.41	CrO_x/Al_2O_3	86	0.36	53.8	41.1	0	0.9	3.8	99.6
$0.7Cu/Al_2O_3$	124	0.42	$CrO_x/0.7Cu/Al_2O_3$	111	0.37	51.8	42.6	0.7	0.9	3.8	99.8
$1.3Cu/Al_2O_3$	123	0.39	$CrO_x/1.3Cu/Al_2O_3$	111	0.36	50.8	43.2	1.3	0.9	3.7	99.9
$2.6Cu/Al_2O_3$	124	0.38	$CrO_x/2.6Cu/Al_2O_3$	103	0.33	50.6	42.2	2.6	0.8	3.7	100
$3.2Cu/Al_2O_3$	113	0.37	$CrO_x/3.2Cu/Al_2O_3$	102	0.32	50.3	41.7	3.2	0.9	3.7	99.8
$6.5Cu/Al_2O_3$	95	0.31	$CrO_x/6.5Cu/Al_2O_3$	88	0.30	49.5	39.4	6.5	0.8	3.5	99.7

2.2. Characterization of supports and catalysts

Porous structure of the synthesized samples was studied using low-temperature N_2 adsorption ($-196\ °C$) on an automatic gas-adsorption analyzer "TriStar 3020" ("Micrometrics", USA). To determine the specific surface area (S_{BET}), the isotherms of N_2 adsorption were aligned in the range of relative pressures P/P_0 from 0.05 to 0.30 using the multi-point BET method. The curves of pore size distribution were calculated using the BJH-Adsorption with analysis of adsorption branch of adsorption-desorption N_2 isotherms. All measurements were carried out over the samples with a mass of 100–120 mg preliminary degassed in vacuum for 2 h at 200 °C.

The effect of the modifier on phase transition of pseudoboehmite in modified and unmodified supports was studied using the simultaneous thermal analysis method on the STA 449 F1 Jupiter equipped with mass-spectrometer QMS 403D Aëolos (Netzsch, Germany). The samples with the mass of 5–10 mg were heated with a rate of 10 °C/min in air in the temperature range of 30–800 °C.

Phase composition of supports and catalysts was studied using X-ray diffraction analysis on the Miniflex 600 ("Rigaku Corporation", Japan) with a CuKα radiation (γ = 1.5418 Å) equipped with monochromator. The analysis of the results was carried out on the basis of literature data and PCPDFWIN database. Chemical composition of the catalysts was determined by X-ray fluorescent analysis on the XRF–1800 spectrometer ("Shimadzu", Japan).

The studies of chemical state of copper and active component were carried out using diffuse reflection electron microscopy on the Evolution 600 spectrometer ("Thermo Scientific", USA) with a basic line of the spectrum of freshly precipitated $BaSO_4$ as well as the Raman spectroscopy under conditions of the environment using confocal Raman microscope inVia (Renishaw, UK) with an excitation line at 525 nm.

The study of the reductive ability of the synthesized supports and catalysts was carried out using the temperature-programmed reduction with hydrogen (H_2-TPR). The analysis was carried out using the chemisorption analyzer ChemiSorb 2750 ("Micromeritics", USA) with the thermal conductivity detector (TCD signal). The heating rate and the flow rate of the Ag–H_2 mixture (10 %vol. H_2) were 10 °C/min and 20 ml/min, respectively.

2.3. Testing of catalytic properties of the samples

Catalytic testing of the synthesized catalysts in isobutane dehydrogenation was carried out in a kinetic mode at 540 °C with a low contact time (0.3 s) to keep isothermal mode and conversion below the thermodynamic equilibrium (Salaeva et al., 2019) that allowed suppressing the carbon deposition and minimizing the catalyst deactivation. The flow unit with a quartz reactor (i.d. = 15 mm) and a fixed catalyst bed was used. The catalyst sample with a volume of 0.75 ml and a mass of 0.49–0.56 g was mixed with quartz (~1.2 ml). The experiment was carried out during 4 h in a cyclic mode. Reaction mixture 15% i-C_4H_{10} (pure: 99.9, LLC "Pure gases", Novosibirsk) in N_2 (LLC "Pure gases", Novosibirsk) with a rate of 9 L/h (1.35 i-C_4H_{10} /7.65 N_2; GHSV = 2700 h^{-1}) was passed through the fixed catalyst bed with the particle diameter of 0.1–0.25 mm to avoid the diffusion limitations. The catalysts were subjected to regeneration in air at 540 °C for 20 min and reduction in H_2 + N_2 (15% H_2) mixture at the same temperature for 3 min. Analysis of the products was carried out using the online gas chromatograph Chromatec-Crystall 5000.2 with a thermal conductivity detector (TCD), two flame ionization detectors (FID) on the capillary column Varian CP-Al_2O_3/Na_2SO_4 (50 m, 130 °C). The following reaction products were analyzed: methane, ethane, ethylene, propane, propylene, i-butane, n-butane, trans-butene-2,

butane-1, i-butene, and cis-2-butene. The material balance for carbon was above 97% in all experiments. The conversion and selectivity values were calculated as follows:

$$X = \left(1 - C_{i\text{-}butane(out)}/C_{i\text{-}butane(in)}\right) * 100\% \qquad (1)$$

$$S = \left(C_{i\text{-}isobutylene}/\left(C_{i\text{-}butane(in)} - C_{i\text{-}butane(out)}\right)\right) * 100\% \qquad (2)$$

where $C_{i\text{-}butane(in)}$ is the isobutane concentration before reactor, $C_{i\text{-}butane(out)}$ and $C_{i\text{-}butylene(out)}$ are concentrations of isobutane and isobutylene, respectively, after reactor.

3. Results and discussion

3.1. Characterization of supports and catalysts

The porous structure of the supports and catalysts on the basis thereof was studied using low-temperature N_2 adsorption. Fig. 1 shows the isotherms of N_2 adsorption-desorption and pore size distributions for the synthesized supports (Fig. 1a,c) and catalysts (Fig. 1b,d). The presence of a hysteresis loop on the isotherms of N_2 adsorption-desorption in the range of relative pressures from 0.5 to 1.0 for all synthesized samples evidences their mesoporous structure. Pore size distributions show that all samples are characterized by the presence of mesopores with a width of 3–20 nm.

The porous structure of the unmodified Al_2O_3 support (Fig. 1c), prepared by pseudoboehmite calcination at 750 °C, is characterized by the bimodal pore size distribution: narrow mesopores with a width of 2–8 nm and larger mesopores with a width of 5–20 nm. For the Cu-modified supports, the shape of the hysteresis loop in the isotherms changes as compared to the one for Al_2O_3 and is accompanied by the shifting of the loop towards lower relative pressures and a decreasing of the loop width in the range of 0.9–1.0. The pore size distributions for 0.7Cu/Al_2O_3 and 1.3Cu/Al_2O_3 supports differ from the one for Al_2O_3 due to a shifting of the large pores with sizes of 7–25 nm to smaller pore sizes, while retaining the amount of narrow mesopores with sizes of 2–5 nm. The modified supports with Cu loading of 2.6–6.5% wt are characterized by monomodal pore size distribution due to a significant shift of larger pores to smaller sizes. Thus, Cu modifier facilitates the formation of more narrow mesopores. For Cu-modified supports, the S_{BET} increases up to 123–124 m^2/g (Table 1) as compared with the unmodified alumina support (115 m^2/g). However, the subsequent increase of Cu content up to 6.5% wt results in a decrease of the S_{BET} to up to 95 m^2/g and a narrowing of the pore volume to up to 0.30 cm^3/g that can be connected with the filling of the pores with an excess of Cu compounds.

For all catalysts (Fig. 1b), a slight shift of the hysteresis loop towards higher relative pressures (0.65–1.0) in the N_2 adsorption-desorption isotherms and corresponding insignificant increase of the size of mesopores are observed (Fig. 1d). A decrease of S_{BET} and pore volume for the catalysts (Table 1) as compared to supports indicates a distribution of active component inside the pores of the support. Changing of the porous structure of the catalysts as compared to the supports (mainly, widening of the pores) is a result of peptization of alumina support by chromic acid in the impregnation solution. It is noteworthy that the largest changing of pore size distribution and the highest decrease of S_{BET} is observed for the catalysts based on unmodified alumina support, while the changing of porous structure of the Cu-modified samples is lower that indicates an additional stabilization of the structure of alumina support by the Cu modifier.

The peculiarities of structure formation for the supports and the effect of Cu modifier on the transformation of pseudoboehmite into γ-Al_2O_3 phase was studied by TG-DSC analysis. Fig. 2 shows the results of thermal analysis for initial pseudoboehmite and the
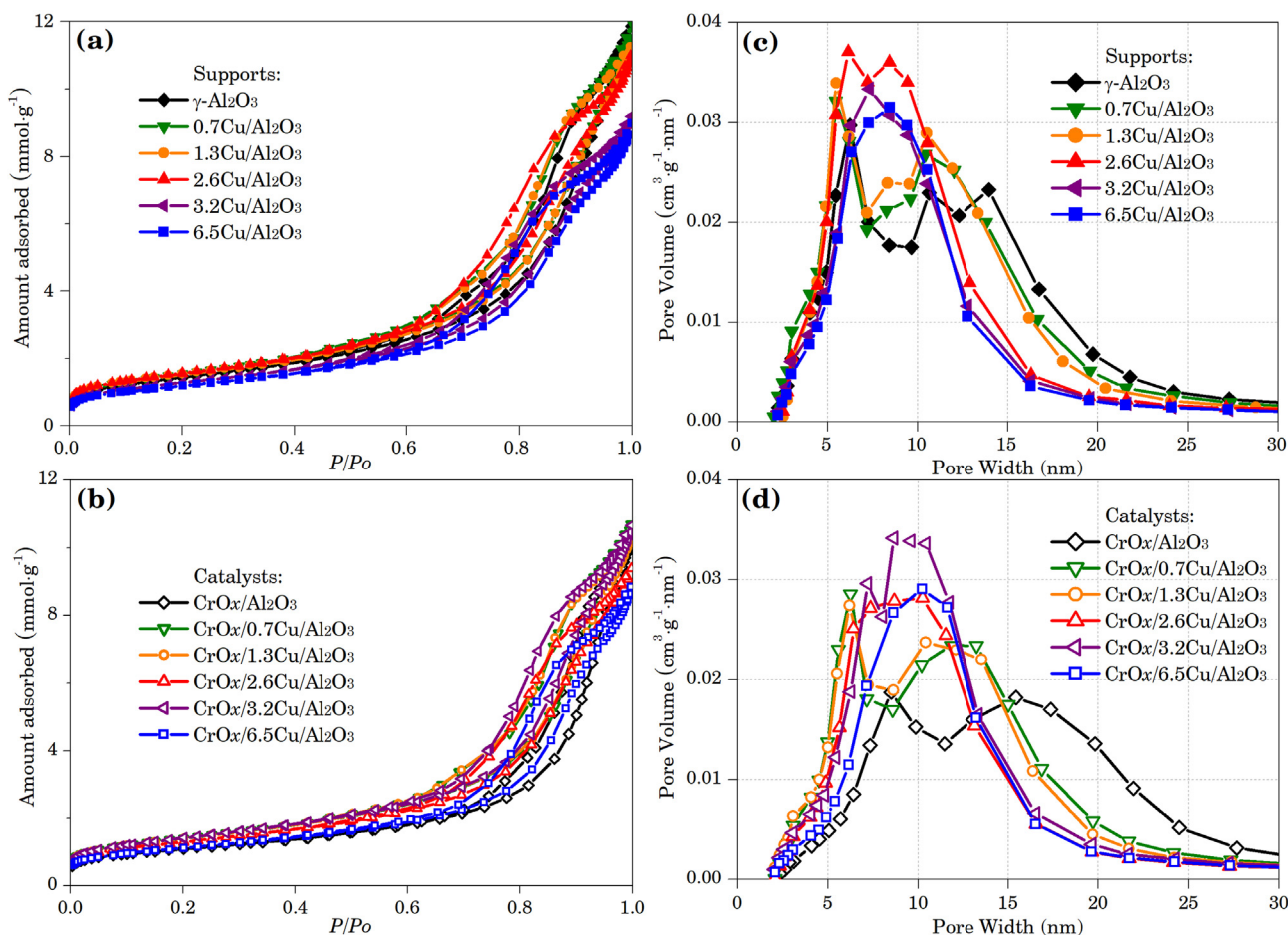
Fig. 1. Low-temperature N_2 adsorption-desorption isotherms (a,b) and the corresponding pore size distributions (c,d) for supports and alumina-chromia catalysts.
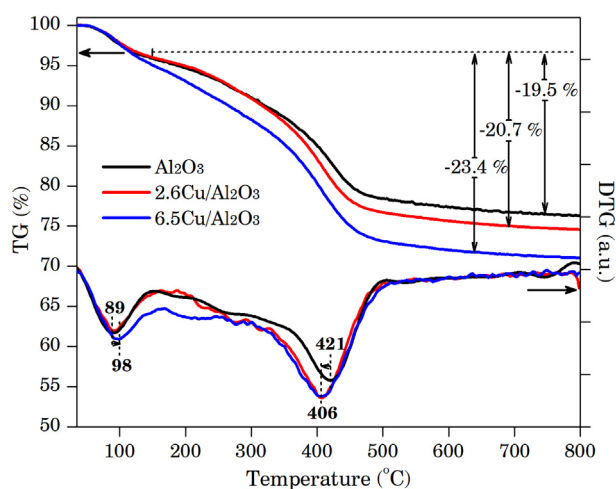

Fig. 2. TG-DSC curves for dried supports.

one after impregnation with an aqueous solution of copper nitrate (the samples with Cu contents of 2.6 and 6.5 wt dried at 120 °C for 12 h). The mass loss at 89–98 °C indicates desorption of physically bound water. The absence of the expressed peaks in the range of 200–300 °C indicates the absence or low content of aluminum trihydroxides (gibbsite, bayerite) in pseudoboehmite structure (Zykova et al., 2016; Redaoui et al., 2017; Mukhamed'yarova et al., 2019). The mass loss in the range from 300 to 500 °C with

a wide endothermic peak at 406–421 °C evidences the pseudoboehmite transformation into γ-Al_2O_3 (Zykova et al., 2016). It is noteworthy that the introduction of Cu leads to a shifting of the pseudoboehmite-to-γ-Al_2O_3 phase transition towards lower temperatures. Thus, the introduction of Cu into the alumina precursor results in the formation of γ-Al_2O_3 phase at lower temperatures. This may result in the formation of more narrow pores in the modified supports as compared to the unmodified one.

Phase composition of the catalysts, states of the alumina-supported active component and modifier were studied using XRD, UV–vis, and Raman spectroscopy methods. Fig. 3 shows the X-ray patterns for the Al_2O_3 and 6.5Cu/Al_2O_3 supports as well as the alumina-chromia catalysts. All samples are characterized by the presence of a number of reflections attributed to γ-Al_2O_3 phase (card No. 00-050-0741). The absence of reflections of α-Cr_2O_3 (card No. 01-078-5434) and CuO (card No. 000–45-0937) phases evidences the stabilization of Cu and Cr compounds in a highly dispersed X-ray amorphous state.

It is noteworthy that there are differences in the intensity and width of reflections at the 2θ values of 36.7°, 45.9° and 66.8° in the X-ray patterns for the unmodified and Cu-modified alumina-chromia catalysts. According to PCPDFWIN database and the results by Kim et al. (2001), the presence of reflections in this range can be assigned to the formation of phases of aluminum-copper spinels (CuAl$_2$O$_4$ (card No. 33-0448)). However, the low intensity of the reflections and their close positions as compared to those of the γ-Al_2O_3 phase does not allow making a univocal conclusion on the presence of individual phase of the aluminum-copper spinel. Along with that, an increase of the cubic cell lattice parameter,
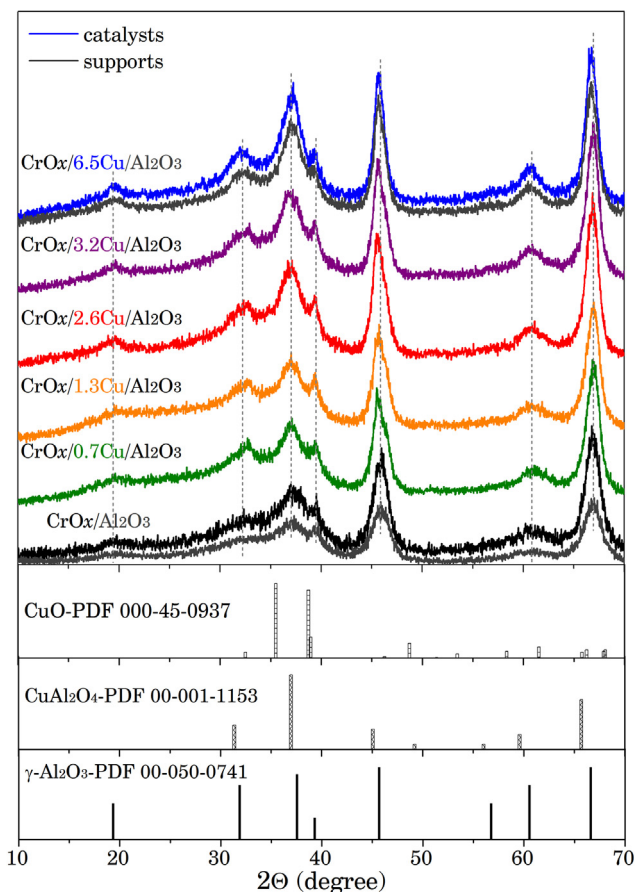
Fig. 3. X-ray patterns of Al$_2$O$_3$, 6.5Cu/Al$_2$O$_3$ supports and alumina-chromia catalysts.

Fig. 4. UV–vis spectra of the supports (a) and catalysts (b).

Table 2
Results of XRD analysis of the synthesized supports and alumina-chromia catalysts.

Sample	Particle size (CSR*), nm			a, Å
	36.7° (3 1 1)	45.9° (4 0 0)	66.8° (4 4 0)	
Al$_2$O$_3$	3.4	5.1	6.4	7.9058
6.5Cu/Al$_2$O$_3$	2.7	6.7	7.0	7.9347
CrO$_x$/Al$_2$O$_3$	3.5	5.3	6.5	7.9062
CrO$_x$/0.7Cu/Al$_2$O$_3$	3.5	5.4	6.3	7.9067
CrO$_x$/1.3Cu/Al$_2$O$_3$	2.9	5.5	6.4	7.9115
CrO$_x$/2.6Cu/Al$_2$O$_3$	3.8	5.8	6.8	7.9298
CrO$_x$/3.2Cu/Al$_2$O$_3$	3.9	6.1	7.0	7.9306
CrO$_x$/6.5Cu/Al$_2$O$_3$	4.0	6.9	7.4	7.9384

* CSR is a coherent scattering region for γ-Al$_2$O$_3$ calculated according to Sherrer's equation.

a, for γ-Al$_2$O$_3$ phase (Table 2) from 7.9058 to up to 7.9384 Å occurs at an increase of Cu content that does not indicate the formation of a new phase, but rather distortion of the structure of γ-Al$_2$O$_3$ phase as a result of incorporation of copper cations. Additionally, the increased values of crystallite sizes (Table 2) for Cu-modified catalysts confirm the influence of copper on the formation of the γ-Al$_2$O$_3$ structure during the pseudoboehmite transformation. Thus, according to XRD data, Cu ions are incorporated into the structure of alumina support, while it is not possible to reliably identify the stoichiometry of the surface phase formed, since the reflections are poorly resolved.

The UV–vis method was used to describe in more details the surface states of active component and modifier in the supports and catalysts (Fig. 4). Practical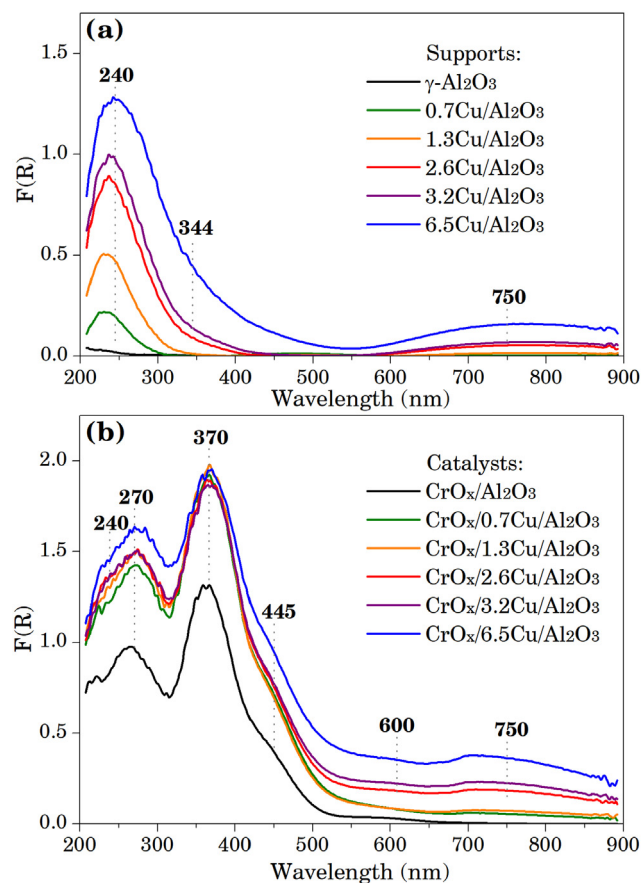ly no absorption is observed for pure Al$_2$O$_3$ in the range of 200–900 nm. For Cu-modified supports (Fig. 4a), an intensive absorption band is observed in the range of 240 nm, and the intensity of this band increases as the amount of the introduced Cu grows. This absorption can be assigned to O → Cu^{2+} charge transfer in octahedral environment (Yashnik et al., 2015; Yamamoto et al., 2002). For the supports containing from 2.6 to 6.5% wt Cu, a shoulder is observed in the range of 344 nm. According to Ref. (Yamamoto et al., 2002), this evidences the presence of CuAl$_2$O$_4$ phase with the ligand-to-metal charge transfer for tetrahedrally coordinated Cu^{2+}. A weak absorption band in the range of 700–800 nm indicates the d-d transition of isolated Cu^{2+} ions with the tetragonally distorted octahedral environment (Yashnik et al., 2015). This band is more characteristic for the support with 6.5% wt Cu that indicates the formation of Cu (II) oxide in the sample.

Two main absorption bands with the maxima at 270 and 370 nm are observed in the UV–vis spectra of the as-prepared CrO$_x$ catalysts (Fig. 4b) and characterize the presence of monochromate species and the O → Cr^{6+} electronic transition with a tetrahedrally coordinated Cr(VI) (Cavani et al., 1996; Merk et al., 2018; Martino et al., 2018). An increase in the intensity of the absorption bands at 270 nm for the modified catalysts is connected with both the contribution of the absorption band at 240 nm (O → Cu^{2+}) and the increase in the amount of Cr(VI) species. A significant increase in the intensity of the absorption band at 370 nm for all Cu-modified catalysts as compared to unmodified CrO$_x$/Al$_2$O$_3$ catalysts indicates the increase in the share of Cr(VI) species. However, the intensities of the bands at 270 and 370 nm decrease for CrO$_x$/3.2-Cu/Al$_2$O$_3$ and CrO$_x$/6.5Cu/Al$_2$O$_3$ catalysts (subtraction spectra are not shown for clarity). According to the data in Refs. (Cavani et al., 1996; Weckhuysen et al., 1997; Cutrufello et al., 2005), a

shoulder at 445 nm is connected with the presence of dichromate species.

A doublet at 445 and 600 nm is observed for all catalysts and evidences the d–d transition of Cr^{3+} in the octahedral environment (Bugrova et al., 2015; Shee and Sayari, 2010). More resolved absorption of these bands is observed for $CrO_x/6.5Cu/Al_2O_3$ that indicates the increase in the share of Cr(III) in the catalyst. An intensity growth for absorption band in the range of 700–800 nm for the catalysts with the copper content of 2.6–6.5% wt, is probably caused by the presence of Cu^{2+} ions in these samples. An increase in the intensity of these bands as compared to those over the corresponding Cu-modified supports indicates a redistribution of Cu when the active component is introduced, i.e. partial leaching of Cu modifier in the acidic impregnating solution.

Fig. 5 shows the Raman spectra for the studied catalysts. The Al_2O_3 and Cu-modified supports do not show high absorption in the range considered (the corresponding spectra are not shown), while the catalysts are characterized by an intensive absorption of various Cr species in the range of 700–1050 cm^{-1}.

For CrO_x/Al_2O_3 catalysts, the main band at ~860 cm^{-1} is assigned to symmetric vibrations of isolated tetrahedral surface-chromate species that interact with the alumina support (Fridman et al., 2016; Ma et al., 2011; Hardcastle and Wachs, 1988) and/or dimeric chromium oxide species (Mindru et al., 2016). For all catalysts, the vibration in the range of ~883 cm^{-1} indicates the presence of hydrated surface monochromate species (Fridman et al., 2016). The presence of shoulders at ~784, ~822 and ~931, ~987 cm^{-1} is connected, respectively, with weak vibrations of Cr–O–Cr groups (Vuurman and Wachs, 1992; Dines and Inglis, 2003), chromates with high polymerization degree (Hardcastle and Wachs, 1988), terminal CrO_3 groups (Salaeva et al., 2019; Yim and Nam, 2004), and crystalline forms of CrO_3 (Vuurman
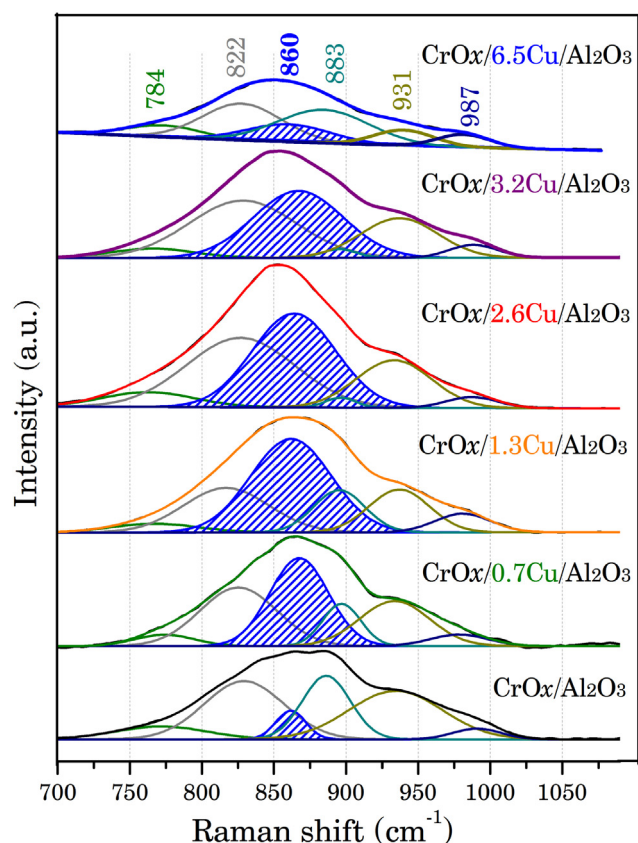
and Wachs, 1992; Oskam et al., 1990). There are no vibrations at ~537 and ~600 cm^{-1} attributed to crystalline Cr_2O_3 nanoparticles (Bugrova et al., 2019). The results for the $CrO_x/2.6Cu/Al_2O_3$ sample indicate the increased fraction of mono- and dimeric chromium oxide species (Yim and Nam, 2004) confirmed by the UV–vis data (Fig. 4, absorption band at 445 nm). For the $CrO_x/6.5Cu/Al_2O_3$ catalyst, the halo in the range of 600–700 nm is observed and can be attributed to dispersed copper oxide (Luo et al., 2005).

Thus, the Raman data show that in the studied catalysts Cr predominantly exists in a hexavalent state. Introduction of 2.6% wt Cu results in the increase of the fraction of Cr(VI) in the catalysts. The subsequent increase of the Cu content to up to 6.5% wt results in the decrease in Cr(VI) content. The hexavalent Cr exists on the catalyst surface predominantly as mono- and dichromate species.

The XRD, UV–vis and Raman data show that the active component exists in a poorly crystalline X-ray amorphous state predominantly in the form of mono- and dichromate species (Cr^{6+}) with a small amount of Cr(III). Cu modifier, in its turn, is distributed in the support structure as incorporated Cu^{2+} cations. The sample with 6.5 %wt Cu may contain highly dispersed copper oxides.

The H_2-TPR method was used to study the peculiarities of reduction of modified supports and the catalysts. Fig. 6 and Table 3 show the H_2-TPR profiles of synthesized supports and catalysts and the corresponding amount of hydrogen consumed during the TPR experiments. The unmodified γ-Al_2O_3 support is characterized by low H_2 consumption (83 μmol/g) at temperatures above 500 °C that is probably connected with a partial reduction of the alumina surface accompanied by the formation of oxygen vacancies (Rodemerck et al., 2016).

The supports that contain up to 2.6% wt Cu are characterized by poorly resolved H_2 consumption peak in the range of 300–600 °C. However, the TPR profiles for the samples 2.6Cu/Al_2O_3, 3.2Cu/Al_2O_3 and 6.5Cu/Al_2O_3 have better resolved peaks at 300, 282 and 271 °C, respectively, that may evidence a reduction of copper cations incorporated into the alumina support (Kim et al., 2001;
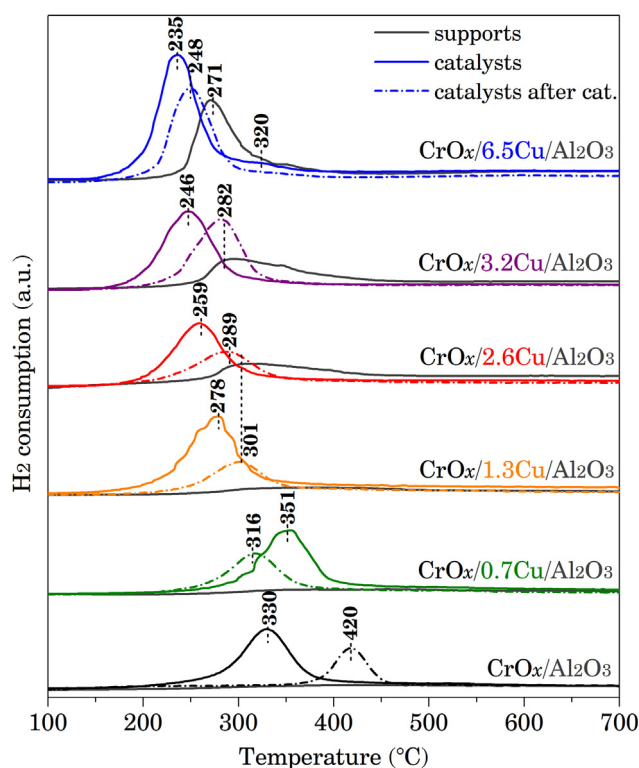

Fig. 5. Raman spectra of the synthesized catalysts.

Fig. 6. H_2-TPR profiles of synthesized supports and catalysts.

Table 3
Amount of hydrogen consumed during the H_2-TPR experiments by supports and catalysts.

Sample	n H_2, µmol/g			
	Supports	Fresh catalysts	$\Delta H_{2(cat-sup)}$	After catalysis
CrO_x/Al_2O_3	83	499	416	357
$CrO_x/0.7Cu/Al_2O_3$	118	535	417	413
$CrO_x/1.3Cu/Al_2O_3$	175	590	415	437
$CrO_x/2.6Cu/Al_2O_3$	255	720	465	445
$CrO_x/3.2Cu/Al_2O_3$	343	722	379	547
$CrO_x/6.5Cu/Al_2O_3$	550	820	270	631

He et al., 2006) or the presence of a highly dispersed $CuAl_2O_4$ spinel (Yashnik et al., 2015). Lower temperature and higher intensity of the H_2 consumption peak for the support containing 6.5% wt Cu may evidence the reduction of dispersed copper oxide CuO (Yashnik et al., 2015; Luo et al., 2005). With that, for this support the high-temperature sloping shoulder at ~320 °C also retains that indicates the presence of Cu^{2+} cations in the structure of alumina support.

The unmodified CrO_x/Al_2O_3 catalyst is characterized by a single peak of hydrogen consumption with a maximum at 330 °C that, according to the literature data (Bugrova and Mamontov, 2018; He et al., 2006; Hosseini et al., 2014), is attributed to the reduction of Cr^{6+} to Cr^{3+}. Introduction of 0.7% wt Cu insignificantly changes the temperature profile for the catalyst accompanied by a shifting of the hydrogen consumption peak from 330 to 351 °C. For other catalysts containing 1.3–6.5% wt Cu, a significant changing of the temperature profile occurs and is accompanied by a decreasing of the reduction temperature of the main peak from 351 to 235 °C. This may evidence the promotion effect of Cu on the reducibility of highly dispersed surface Cr species or weaker interaction between Cu-modified support and CrO_x species.

The difference in the amount of H_2 consumed between the corresponding catalyst and support ($\Delta H_{2(cat-sup)}$, Table 3) for CrO_x/Al_2O_3 and Al_2O_3, $CrO_x/0.7Cu/Al_2O_3$ and $0.7Cu/Al_2O_3$, and $CrO_x/1.3$-Cu/Al_2O_3 and $1.3Cu/Al_2O_3$ pairs has close values. However, an increase in the amount of the introduced Cu modifier to up to 2.6% wt results in the subsequent shifting of the main TPR peak towards lower temperatures, a decrease in the peak area, and an increase in the difference of the H_2 consumed by the catalyst and support to up to 465 µmol/g that indicates a significant increase in the share of the redox Cr^{6+}. For the catalysts with Cu content of 3.2 and 6.5% wt, a decrease of the $\Delta H_{2(cat-sup)}$ value is observed that indicates a reduction of the share of Cr^{6+}. This is consistent with the UV–vis results (since the absorption of Cr^{3+} is observed in the spectra for these catalysts) and Raman spectroscopy data.

It is noteworthy that for the samples with copper content of 2.6, 3.2 and 6.5% wt, a difference in the TPR profiles between the supports and catalysts consists in the absence of the main reduction peak for the support in the profile for the catalyst, and only its high-temperature region partially retains (e.g., for the sample with 6.5% wt Cu there is no peak at 271 °C in the profile of the catalyst, while the shoulder at 320 °C retains). This indicates Cu redistribution during the deposition of the active component, and the probable formation of mixed or contacting phases of Cu and Cr takes place. The co-reduction of these phases proceeds at lower temperatures as compared to the supports and the unmodified CrO_x/Al_2O_3 catalyst.

Thus, based on the TPR data it is possible to conclude that Cu modifier facilitates an easier reduction of Cr^{6+} species (Yashnik et al., 2015; Yamamoto et al., 2002). The maximal amount of Cr^{6+} estimated on the basis of $\Delta H_{2(cat-sup)}$ value, is observed for the sample with 2.6% wt Cu. The subsequent increase in the amount of Cu modifier results in a decrease in Cr^{6+} content.

3.2. Catalytic properties in reaction of isobutane dehydrogenation

Catalytic properties of the synthesized catalysts were studied in the isobutane dehydrogenation in a kinetic mode at the isobutane conversion of 4.6–19.7% that was below the thermodynamic equilibrium conversion for dehydrogenation-hydrogenation at 540 °C (Sanfilippo and Miracca, 2006). The results obtained are represented as a conversion (X, %) and selectivity (S, %) dependence on the dehydrogenation time during the six cycles (Fig. 7a), with the oxidative regeneration and reductive activation being carried out between the cycles similar to the Catofin process (Pat. WO, 2018).

All catalysts show close and high selectivities (97–99%) that are determined by relatively low conversion values in the kinetic mode and the absence or very low impact of the carbon deposition processes that was confirmed by the TG-STA data during the study of the catalysts cooled down in the inert atmosphere after six dehydrogenation cycles. For the catalysts with 3.2 and 6.5% wt Cu, the selectivity gradually decreases from cycle to cycle that indicates a negative effect of higher amounts of Cu modifier on the formation of selective dehydrogenation sites in the catalyst.

The reference catalyst CrO_x/Al_2O_3 shows the 10.3% conversion during the first cycle, however, after the regeneration-reduction treatment, the conversion increases to up to 13.3–14.0% during the subsequent five cycles of the dehydrogenation reaction. This effect indicates the run-in of the catalyst without subsequent deactivation that can be connected with the redistribution of various Cr species on the catalyst surface under the influence of oxidative and reductive media.

The modified catalysts with Cu content of 0.7–2.6% wt are more active during six catalytic dehydrogenation cycles as compared to the unmodified one. The catalysts $CrO_x/0.7Cu/Al_2O_3$ and $CrO_x/1.3$-Cu/Al_2O_3 show the conversion values of 15.9–16.5% at the first cycle that slightly increases after the oxidative regeneration and reduction and retains at the level of 15.3–17.2% up to the sixth cycle. The catalyst with Cu content of 2.6% wt is characterized by the highest conversion values at the first and subsequent cycles (18–18.4%) that can be caused by the highest fraction of monomeric and dimeric Cr(VI) species in the catalyst shown by Raman spectroscopy (Fig. 5).

For the catalysts with 3.2 and 6.5% wt Cu, the conversion at the first catalytic cycle is 15.8 and 10.0%, respectively, while during the subsequent catalytic cycles, their activity rapidly decreases (up to 11.3% and 4.6%, respectively). A reduction of the activity of these samples as compared to those with 2.6% wt Cu can be connected with the decrease of the total amount of Cr(VI) (according to TPR data) as well as with Cr transition from monomeric species towards less active dimeric and polymeric ones. For these catalysts, the oxidative and reductive treatments between the dehydrogenation cycles result in an activity decrease that can be caused by the presence of poorly crystalline CuO in the samples and the fact that the treatments can significantly affect the Cr distribution, e.g., due to the formation of phases that contain both Cu and Cr.

Thus, the catalytic activity of the alumina-chromia catalysts is a function of the Cu modifier content (Fig. 7b) and increases as the Cu content grows to up to 2.6% wt The subsequent increase in Cu content results in a decrease of activity and stability of the catalysts. The activity is mainly determined by the amount and state of redox Cr(VI) species. The introduction of moderate amounts of Cu modifier (up to 2.6% wt Cu) increases both the fraction of redox Cr(VI) species and stabilization of mononuclear and dimeric Cr(VI) species, and their reduction prior to the catalytic process leads to the formation of mononuclear and dimeric Cr(III) species and to the corresponding increase of the activity in the isobutane dehydrogenation.

The study of the catalysts after six catalytic cycles using H_2-TPR method (Fig. 6) allows estimating the fraction of the redox Cr
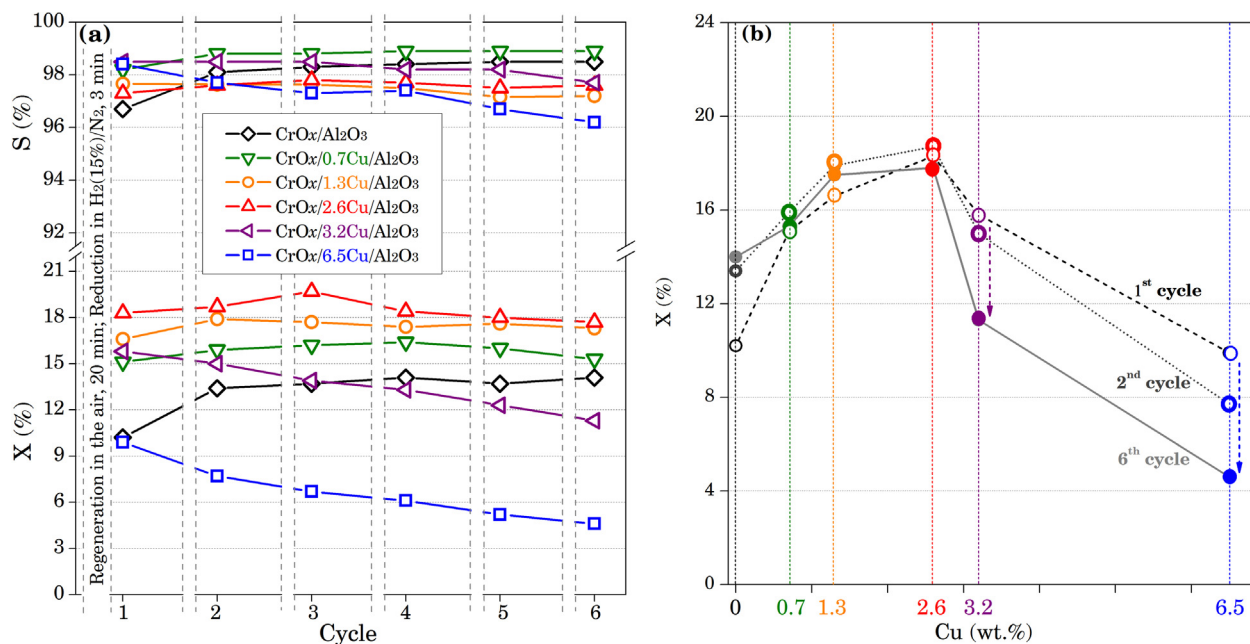
Fig. 7. Dependence of isobutane conversion and selectivity towards isobutylene during the isobutane dehydrogenation at 540 °C over the synthesized alumina-chromia catalysts during six cycles (a), and dependencies of isobutane conversion at the first, second and sixth cycles on the content of Cu modifier in the catalysts (b).
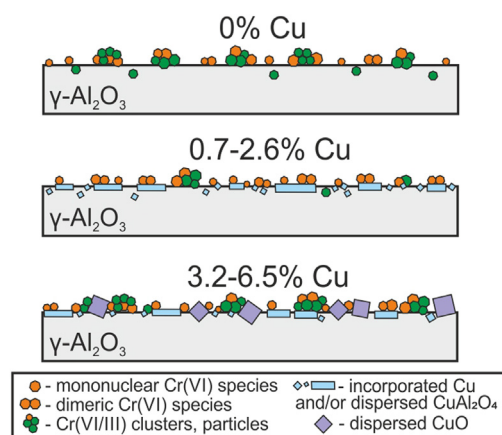

Fig. 8. A scheme of active surface formation of preoxidized Cu-modified alumina-chromia catalysts.

species in the aged catalysts. For CrO_x/Al_2O_3, a decrease of H_2 consumption occurs along with a significant shift (by ~90 °C) towards the high-temperature region that may be connected both with increasing dispersion of CrO_x species on the alumina surface and with the formation of mixed chromia–alumina phases. The H_2-TPR profiles show that the introduction of copper results in a lower shift of the H_2 consumption peak maximum towards the high-temperature region that decreases from 35 to 10 °C as the amount of the introduced Cu grows. It is noteworthy that after six catalytic cycles, the $CrO_x/2.6Cu/Al_2O_3$ sample retains a higher amount of redox Cr(VI) species (Table 3) that is caused by the predominance of mono- and dimeric Cr species on the surface of as-prepared catalyst (Fig. 5).

Based on the results obtained by a complex of physical-chemical methods, a scheme of active surface formation of Cu-modified alumina-chromia catalysts is proposed (Fig. 8). For the catalysts with Cu content below 2.6% wt, the formation of highly dispersed Cu and active component in the form of mononuclear species is observed. The catalyst with 2.6 wt Cu shows the highest

conversion that may be caused by the initiation of formation of highly dispersed surface spinels and redistribution of active component to yield higher fraction of dimeric Cr species.

Further increase in Cu content yields surface CuO phase along with incorporated Cu and/or highly dispersed $CuAl_2O_4$ that is confirmed by the UV–vis (Fig. 4a) and H_2-TPR (Fig. 6) data. Hence, for $CrO_x/3.2Cu/Al_2O_3$ and $CrO_x/6.5Cu/Al_2O_3$ samples, a decrease of the fraction of dimeric Cr species (Fig. 5) and the appearance of Cr(III) species (Fig. 4b) is observed resulting in conversion decrease at the second catalytic cycle (Fig. 7a).

4. Conclusions

Thus, the introduction of Cu modifier was shown to enhance the activity of CrO_x/Al_2O_3 catalysts in the fixed-bed isobutane dehydrogenation into isobutylene. Introduction of 0.7–6.5% wt Cu leads to the changing of the distribution of CrO_x species on the support surface, significant growth of the amount of Cr^{6+} species, and a decrease of the catalyst reduction temperature from 330 to up to 235 °C. Cu modifier was shown to stabilize on the support surface predominantly as copper cations incorporated into the structure of alumina support, however, the increase of Cu content to up to 3.2 and 6.5% wt leads to the formation of highly dispersed copper oxides.

The highest conversion towards isobutylene in the process of isobutane dehydrogenation into isobutylene has been obtained over the catalyst containing 2.6% wt Cu. The observed effect can be explained by the incorporation of Cu into the alumina structure that results in the stabilization of active component mostly as monomeric and dimeric Cr(VI) species. The reduction of these species prior to the catalytic process leads to the formation of the most active mononuclear and dimeric Cr^{3+} sites. The results obtained are of practical importance for enhanced performance of industrial catalysts for dehydrogenation of light paraffin hydrocarbons.

The increase of Cu content to up to 6.5% wt results in a decrease in the amount of redox Cr(VI) species that decreases both catalyst activity and selectivity. Thus, high content of Cu modifier has a negative influence on the properties of alumina-chromia catalyst

that may play a key role in the exploitation of alumina-chromia catalyst along with Cu-containing heat-generating material in the Catofin process. The addition of Cu onto the catalyst surface may increase the activity, but high amounts of transferred Cu may lead to fast catalyst deactivation.

CRediT authorship contribution statement

A.A. Salaeva: Investigation, Visualization, Writing - original draft. **M.A. Salaev:** Visualization, Writing - review & editing, Formal analysis, Methodology. **G.V. Mamontov:** Writing - review & editing, Methodology, Conceptualization, Project administration, Funding acquisition, Resources.

Declaration of Competing Interest

The authors declare that they have no known competing financial interests or personal relationships that could have appeared to influence the work reported in this paper.

Acknowledgements

References

Bahmani, M., Farahani, B.V., Sahebdelfar, S., 2016. Preparation of high performance nano-sized Cu/ZnO/Al₂O₃ methanol synthesis catalyst via aluminum hydrous oxide sol. Appl. Catal. A. 520, 178–187. https://doi.org/10.1016/j.apcata.2016.04.018.

Beccari, M., Romano, U., 2006. Encyclopaedia of hydrocarbons. Rome: ENI & Istituto della enciclopedia italiana G. Treccani 2, 687–697.

Bekmukhamedov, G.E., Mukhamed'yarova, A.N., Egorova, S.R., Lamberov, A.A., 2016. Modification by SiO2 of alumina support for light alkane dehydrogenation catalysts. Catalysts 6, 1–19. https://doi.org/10.3390/catal6100162.

Bugrova, T.A., Litvyakova, N.N., Mamontov, G.V., 2015. Effect of zirconia additives on the activity of the Cr/SiO₂ catalyst in isobutane dehydrogenation. Kinet. Catal. 56, 758–763. https://doi.org/10.1134/S0023158415060014.

Bugrova, T.A., Mamontov, G.V., 2018. The study of CrOₓ-containing catalysts supported on ZrO₂, CeO₂, and Ce$_x$Zr$_{(1-x)}$O₂ in isobutane dehydrogenation. Kinet. Catal. 59, 143–149. https://doi.org/10.1134/S0023158418020027.

Bugrova, T.A., Dutov, V.V., Svetlichnyi, V.A., Corberan, V.C., Mamontov, G.V., 2019. Oxidative dehydrogenation of ethane with CO₂ over CrOₓ catalysts supported on Al₂O₃, ZrO₂, CeO₂ and Ce$_x$Zr$_{1-x}$O₂. Catal. Today 333, 71–80. https://doi.org/10.1016/j.cattod.2018.04.047.

Cabrera, F., Ardissone, D., Gorriz, O.F., 2008. Dehydrogenation of propane on chromia/alumina catalysts promoted by tin. Cat. Tod. 2008 (133–135), 800–804. https://doi.org/10.1016/j.cattod.2007.12.039.

Cavani, F., Koutyrev, M., Trifirò, F., Bartolini, A., Ghisletti, D., Iezzi, R., Santucci, A., Del Piero, G., 1996. Chemical and physical characterization of alumina-supported chromia-based catalysts and their activity in dehydrogenation of isobutane. J. Cat. 158, 236–250. https://doi.org/10.1006/jcat.1996.0023.

Cheng, M., Zhao, H., Yang, J., Zhao, J., Yan, L., Song, H., Chou, L., 2019. Synthesis and catalytic performance of a dual-sites Fe–Zn catalyst based on ordered mesoporous Al₂O₃ for isobutane dehydrogenation. Catal. Lett. 149, 1326–1336. https://doi.org/10.1007/s10562-019-02686-x.

Cutrufello, M.G., De Rossi, S., Ferino, I., Monaci, R., Rombi, E., Solinas, V., 2005. Preparation, characterisation and activity of chromia-zirconia catalysts for propane dehydrogenation. Thermochim. Acta 434, 62–68. https://doi.org/10.1016/j.tca.2005.01.017.

Dines, T.J., Inglis, S., 2003. Raman spectroscopic study of supported chromium(VI) oxide catalysts. Phys. Chem. Chem. Phys. 5, 1320–1328. https://doi.org/10.1039/B211857B.

Dong, A.-H., Wang, K., Zhu, S.-Z., Yang, G.-B., Wang, X.-T., 2017. Facile preparation of PtSn-La/Al₂O₃ catalyst with large pore size and its improved catalytic performance for isobutane dehydrogenation. Fuel Process. Technol. 158, 218–225. https://doi.org/10.1016/j.fuproc.2017.01.004.

Fridman, V.Z., 2010. Pathways of light compounds formation during propane and isobutane dehydrogenation on Al-Cr catalysts. Appl. Catal. A: General. 382, 139–147. https://doi.org/10.1016/j.apcata.2010.04.026.

Fridman, V.Z., Davydov, A.A., Titievsky, K., 2004. Dehydrogenation of cyclohexanol on copper-containing catalysts: II. The pathways of the cyclohexanol dehydrogenation reaction to cyclohexanone on copper-active sites in

oxidation state Cu⁰ and Cu⁺. J. Catal. 222, 545–557. https://doi.org/10.1016/j.jcat.2003.12.016.

Fridman, V.Z., Xing, R., Severance, M., 2016. Investigating the CrOₓ/Al₂O₃ dehydrogenation catalyst model: I. Identification and stability evaluation of the Cr species on the fresh and equilibrated catalysts. Appl. Catal. A 523, 39–53. https://doi.org/10.1016/j.apcata.2016.05.008.

Fridman, V.Z., Xing, R., 2017. Deactivation studies of the CrOₓ/Al₂O₃ dehydrogenation catalysts under cyclic redox conditions. Ind. Eng. Chem. Res. 56, 7937–7947. https://doi.org/10.1021/acs.iecr.7b01638.

Fridman, V.Z., Xing, R., 2017. Investigating the CrOₓ/Al₂O₃ dehydrogenation catalyst model: II. Relative activity of the chromium species on the catalyst surface. Appl. Catal. A: General. 530, 154–165. https://doi.org/10.1016/j.apcata.2016.11.024.

Geilen, F.M.A., Stochniol, G., Peitz, S., Schulte-Koerne, E., 2014. Butenes, Ullmann's Encyclopedia of Industrial Chemistry, Copyright. Wiley VCH Verlag GmbH & Co, KGaA.

Hardcastle, F.D., Wachs, I.E., 1988. Raman spectroscopy of chromium oxide supported on Al₂O₃, TiO₂ and SiO₂: A comparative study. J. Mol. Catal. 46, 173–186. https://doi.org/10.1016/0304-5102(88)85092-2.

He, M., Luo, M., Fang, P., 2006. Characterization of CuO species and thermal solid-solid interaction in CuO/CeO₂-Al₂O₃ catalyst by in-situ XRD, Raman spectroscopy and TPR. J. Rare Earths 24, 188–192. https://doi.org/10.1016/S1002-0721(06)60091-4.

Hosseini, Z.S., Mortezaalia, A., Iraji Zad, A., 2014. Comparative study of the grown ZnO nanostructures on quartz and alumina substrates by vapor phase transport method without catalyst: Synthesis and acetone sensing properties. Sens. Actuators A 212, 80–86. https://doi.org/10.1016/j.sna.2014.03.007.

Kharlamova, T., Sushchenko, E., Izaak, T., Vodyankina, O., 2016. Phase composition, structural peculiarities and catalytic properties of supported MgO-V₂O₅/Al₂O₃ catalysts for oxidative dehydrogenation of propane: Insight into formation of surface Mg-V-O phase. Cat. Tod. 278, 174–184. https://doi.org/10.1016/j.cattod.2016.05.006.

Kim, T.-W., Song, M.-W., Koh, H.-L., Kim, K.-L., 2001. Surface properties and reactivity of Cu/γ-Al₂O₃ catalysts for NO reduction by C₃H₆. Appl. Catal. A: General. 210, 35–44. https://doi.org/10.1016/S0926-860X(00)00801-2.

Lamberov, A.A., Egorova, S.R., Gilmanov, K.K., Kataev, A.N., Bekmukhamedov, G.E., 2017. Pilot tests of the microspherical aluminochromium KDI-M catalyst for iso-butane dehydrogenation. Catal. Ind., 17–22 https://doi.org/10.1134/S2070050417010093.

Lindström, B., Pettersson, L.J., Menon, P.G., 2002. Activity and characterization of Cu/Zn, Cu/Cr and Cu/Zr on γ-alumina for methanol reforming for fuel cell vehicles. Appl. Catal. A 234, 111–125. https://doi.org/10.1016/S0926-860X(02)00202-8.

Liu, Y., Xia, C., Wang, Q., Zhang, L., Huang, A., Ke, M., Song, Z., 2018. Direct dehydrogenation of isobutane to isobutene over Zn-doped ZrO₂ metal oxide heterogeneous catalysts. Catal. Sci. Technol. 8, 4916–4924. https://doi.org/10.1039/C8CY01420E.

Liu, J., Zhou, W., Jiang, D., Wu, W., Miao, C., Wang, Y., Ma, X., 2018. Isobutane dehydrogenation over InPtSn/ZnAl₂O₄ catalysts: Effect of indium promoter. Ind. Eng. Chem. Res. 57, 11265–11270. https://doi.org/10.1021/acs.iecr.8b01728.

Luo, M.-F., Fang, P., He, M., Xie, Y.-L., 2005. In situ XRD, Raman, and TPR studies of CuO/Al₂O₃ catalysts for CO oxidation. J. Mol. Catal. A: Chem. 239, 243–248. https://doi.org/10.1016/j.molcata.2005.06.029.

Ma, R., Hu, P., Jin, L., Wang, Y., Lu, J., Luo, M., 2011. Characterization of CrOₓ/Al₂O₃ catalysts for dichloromethane oxidation. Catal. Today 175, 598–602. https://doi.org/10.1016/j.cattod.2011.04.025.

Martino, G.A., Barzan, C., Piovano, A., Budnyk, A., Groppo, E., 2018. Tracking the reasons for the peculiarity of Cr/Al₂O₃ catalyst in ethylene polymerization. J. Catal. 357, 206–212. https://doi.org/10.1016/j.jcat.2017.11.007.

Matveyeva, A.N., Omarov, S.O., Sladkovskiya, D.A., Murzin, D.Yu., 2019. Experimental studies and kinetic regularities of isobutane dehydrogenation over Ga₂O₃/Al₂O₃. Chem. Eng. J. 372, 1194–1204. https://doi.org/10.1016/j.cej.2019.04.181.

Merk, A.A., Salaev, M.A., Vodyankina, O.V., Mamontov, G.V., 2018. Influence of method of introduction of Cu- and Zn-based modifiers on the properties of chromia–alumina catalysts. Kinet. Catal. 59, 211–217. https://doi.org/10.1134/S0023158418020118.

Mindru, I., Gingasu, D., Patron, L., Marinescu, G., Calderon-Moreno, J.M., Preda, S., Oprea, O., Nita, S., 2016. Copper aluminate spinel by soft chemical routes. Ceram. Int. 42, 154–164. https://doi.org/10.1016/j.ceramint.2015.08.058.

Mukhamed'yarova, A.N., Nesterova, O.V., Boretsky, K.S., Skibina, J.D., Boretskaya, A.V., Egorova, S.R., Lamberov, A.A., 2019. Influence of the obtaining method on the properties of amorphous aluminum compounds Article number 41 Coatings. https://doi.org/10.3390/coatings9010041.

Nawaz, Z., 2015. Light alkane dehydrogenation to light olefin technologies: A comprehensive review. Rev. Chem. Eng. 31, 413–436. https://doi.org/10.1515/revce-2015-0012.

Neri, G., Pistone, A., De Rossi, S., Rombi, E., Milone, C., Galvagno, S., 2004. Ca-doped chromium oxide catalysts supported on alumina for the oxidative dehydrogenation of isobutane. Appl. Catal. A. 260, 75–86. https://doi.org/10.1016/j.apcata.2003.10.002.

Oskam, A., Stufkens, D.J., Vuurman, M.A., 1990. Characterization of CrO3Al₂O₃ catalysts by Raman spectroscopy. J. Mol. Struct. 217, 325–334. https://doi.org/10.1016/0022-2860(90)80371-P.

Otroshchenko, T.P., Rodemerck, U., Linke, D., Kondratenko, E.V., 2017. Synergy effect between Zr and Cr active sites in binary CrZrOₓ or supported CrOₓ/LaZrOₓ: Consequences for catalyst activity, selectivity and durability in non-oxidative

propane dehydrogenation. J. Catal. 356, 197–205. https://doi.org/10.1016/j.jcat.2017.10.012.

Pat. US 2004/0092391 A1, 2004.

Pat. US 2005/0075243 A1, 2005.

Pat. RU 2287366 C1, 2006.

Pat. RU 2350594, 2009.

Pat. RU 2349378, 2009.

Pat. US 20130072739 A1, 2013.

Pat. US 9725380 B2, 2017.

Pat. WO2018144188A1. 2018.

Redaoui, D., Sahnoune, F., Heraiz, M., Raghdi, A., 2017. Mechanism and kinetic parameters of the thermal decomposition of gibbsite Al(OH)$_3$ by thermogravimetric analysis. Acta Phys. Pol., A 131, 562–565.

Rodemerck, U., Kondratenko, E.V., Otroshchenko, T., Linke, D., 2016. Unexpectedly high activity of bare alumina for non-oxidative isobutane dehydrogenation. Chem. Commun. 52, 12222–12225. https://doi.org/10.1039/c6cc06442f.

Rodemerck, U., Stoyanova, M., Kondratenko, E.V., Linke, D., 2017. Influence of the kind of VO$_x$ structures in VO$_x$/MCM-41 on activity, selectivity and stability in dehydrogenation of propane and isobutane. J. Catal. 352, 256–263. https://doi.org/10.1016/j.jcat.2017.05.022.

Rombi, E., Cutrufello, M.G., Solinas, V., De Rossi, S., Ferraris, G., Pistone, A., 2003. Effects of potassium addition on the acidity and reducibility of chromia/alumina dehydrogenation catalysts. Appl. Catal. A. 251, 255–266. https://doi.org/10.1016/S0926-860X(03)00308-9.

Salaeva, A., Salaev, M., Vodyankina, O.V., Mamontov, G., 2019. Synergistic effect of Cu and Zn modifiers on the activity of CrO$_x$/Al$_2$O$_3$ catalysts in isobutane dehydrogenation. Appl. Catal. A 581, 82–90. https://doi.org/10.1016/j.apcata.2019.05.018.

Sanfilippo, D., Miracca, I., 2006. Dehydrogenation of paraffins: Synergies between catalyst design and reactor engineering. Catal. Today 111, 133–139. https://doi.org/10.1016/j.cattod.2005.10.012.

Sattler, J.J., Ruiz-Martinez, J., Santillan-Jimenez, E., Weckhuysen, B.M., 2014. Catalytic dehydrogenation of light alkanes on metals and metal oxides. Chem. Rev. 114, 10613–10653.

Shee, D., Sayari, A., 2010. Light alkane dehydrogenation over mesoporous Cr$_2$O$_3$/Al$_2$O$_3$ catalysts. Appl. Catal. A General 389, 155–164. https://doi.org/10.1016/j.apcata.2010.09.013.

Tasbihi, M., Feyzi, F., Amlashi, M.A., Abdullah, A.Z., Mohamed, A.R., 2007. Effect of the addition of potassium and lithium in Pt-Sn/Al$_2$O$_3$ catalysts for the dehydrogenation of isobutane. Fuel Process. Technol. 88, 883–889. https://doi.org/10.1016/j.fuproc.2007.04.007.

Tian, Y.-P., Bai, P., Liu, S.-M., Liu, X.-M., Yan, Z.-F., 2016. VO$_x$-K$_2$O/γ-Al$_2$O$_3$ catalyst for nonoxidative dehydrogenation of isobutane. Fuel Process. Technol. 151, 31–39. https://doi.org/10.1016/j.fuproc.2016.05.024.

Vuurman, M.A., Hardcastle, F.D., Wachs, I.E., 1993. Characterization of CrO$_3$/Al$_2$O$_3$ catalysts under ambient conditions: Influence of coverage and calcination temperature. J. Mol. Catal. 84, 193–205. https://doi.org/10.1016/0304-5102(93)85052-U.

Vuurman, M.A., Wachs, I.E., 1992. In situ Raman spectroscopy of alumina-supported metal oxide catalysts. J. Phys. Chem. 96, 5008–5016.

Wang, G., Wang, H., Zhang, H., Zhu, Q., Li, C., Shan, H., 2016. Highly selective and stable NiSn/SiO$_2$ catalyst for isobutane dehydrogenation: Effects of Sn addition. ChemCatChem 8, 3137–3145. https://doi.org/10.1002/cctc.201600685.

Wang, G., Li, C., Shan, H., 2016. Catalytic dehydrogenation of isobutane over a Ga$_2$O$_3$/ZnO interface: reaction routes and mechanism. Catal. Sci. Technol. 6, 3128–3136. https://doi.org/10.1039/C5CY01950H.

Wang, G., Sun, X., Niu, X., Meng, F., Wang, F., 2018. Effect of chelating agents on catalytic performance of Cr/γ-Al$_2$O$_3$ dehydrogenation catalysts. Chem. Pap. 72, 921–928. https://doi.org/10.1007/s11696-017-0335-0.

Wang, X.-S., Zhou, G.-L., Chen, Z.-W., Li, Q., Zhou, H.-J., Xu, C.-M., 2018. Enhancing the vanadium dispersion on V-MCM-41 by boron modification for efficient isobutane dehydrogenation. Appl. Catal., A 555, 171–177. https://doi.org/10.1016/j.apcata.2018.02.021.

Weckhuysen, B.M., Verberckmoes, An A., De Baets, A.R., Schoonheydt, R.A., 1997. Diffuse reflectance spectroscopy of supported chromium oxide catalysts: A self-modeling mixture analysis. J. Catal. 166, 160–171. https://doi.org/10.1006/jcat.1997.1518.

Yamamoto, T., Tanaka, T., Kuma, R., Suzuki, S., Amano, F., Shimooka, Y., Kohno, Y., Funabika, T., Yoshida, S., 2002. NO reduction with CO in the presence of O$_2$ over Al$_2$O$_3$-supported and Cu-based catalysts. PCCP 4, 2449–2458. https://doi.org/10.1039/b201120b.

Yashnik, S.A., Kerzhentsev, M.A., Salnikov, A.V., Ismagilov, Z.R., Bourane, A., Koseoglu, O.R., 2015. Cu-Zn-Al-O catalysts for the oxidative desulfurization of dibenzothiophene, a typical sulfur-containing compound of the diesel fraction. Kinet. Catal. 56, 466–475. https://doi.org/10.1134/S0023158415040205.

Yim, S.D., Nam, I.-S., 2004. Characteristics of chromium oxides supported on TiO$_2$ and Al$_2$O$_3$ for the decomposition of perchloroethylene. J. Catal. 221, 601–611. https://doi.org/10.1016/j.jcat.2003.09.026.

Zhang, Y., Zhou, Y., Shi, J., Sheng, X., Duan, Y., Zhou, S., Zhang, Z., 2012. Effect of zinc addition on catalytic properties of PtSnK/γ-Al$_2$O$_3$ catalyst for isobutane dehydrogenation. Fuel Process. Technol. 96, 220–227. https://doi.org/10.1016/j.fuproc.2011.12.040.

Zhang, Y., Zhao, Y., Otroshchenko, T., Lund, H., Pohl, M.-M., Rodemerck, U., Linke, D., Jiao, H., Jiang, G., Kondratenko, E.V., 2018. Control of coordinatively unsaturated Zr sites in ZrO$_2$ for efficient C-H bond activation. Nat. Commun. 9, 1–10. https://doi.org/10.1038/s41467-018-06174-5.

Zykova, A., Livanova, A., Minakova, T., Bugrova, T., Mamontov, G., 2016. Cr2O3/Al2O3 composite catalysts for hydrocarbons dehydrogenation prepared from aluminum nanopowder 030018-1–030018-8 AIP Conf. Proc. 1772.